Catalysis Today 147 (2009) 86–93

Contents lists available at ScienceDirect

Catalysis Today

journal homepage: www.elsevier.com/locate/cattod

Catalytic conversion of syngas into C_2 oxygenates over Rh-based catalysts—Effect of carbon supports

Zhongli Fan, Wei Chen, Xiulian Pan *, Xinhe Bao *

State Key Laboratory of Catalysis, Dalian Institute of Chemical Physics, Chinese Academy of Sciences, 457 Zhongshan Road, Dalian 116023, PR China

ARTICLE INFO

Article history:
Available online 14 April 2009

Keywords:
Syngas conversion
C_2 oxygenates
Rh-based catalyst
Carbon nanotubes

ABSTRACT

Ethanol is considered as a potential alternative synthetic fuel to be used in automobiles or as a potential source of hydrogen for fuel cells. In this paper we first undertake a brief overview of the catalyst development for syngas conversion to C_2 oxygenates over Rh-based catalysts, mainly on the effects of various additives and supports on the activity and selectivity. Then we investigated the effects of carbon materials, which have been rarely studied as supports for Rh-based catalysts in this process. For example, rather well graphitized carbon black, very high surface area CMK-3 and activated carbon (AC) were compared to carbon nanotubes (CNTs), which exhibits a medium level surface area with well defined nanochannels. The CNT-supported catalyst shows a highest overall activity and yield of C_2 oxygenates compared to the other carbon-supported catalysts. The catalysts are characterized by N_2 adsorption–desorption, CO chemisorption, TEM, XRD and TPD. The graphitized structure combined with the tubular morphology of CNTs likely play an important role.

1. Introduction

Ethanol attracts increasing attention as a clean fuel or an additive to gasoline [1,2]. The soaring food price worldwide in 2008 has prompted researchers to seek alternative technologies for ethanol synthesis other than grain fermentation, e.g. from syngas, because syngas can be conveniently manufactured from natural gas, coal and biomass [3]. This process was first patented by Union Carbide Corporation using Rh as a catalyst [4]. Following that, extensive research was carried out. Since single Rh component exhibits a poor activity and mainly leads to formation of hydrocarbon products with methanol being the primary oxygenate, efforts center on improving the dispersion of Rh and modification of Rh with additives and supports in order to selectively synthesize C_2 oxygenates [5–8]. CO hydrogenation is generally considered to involve several steps, including CO dissociation, hydrogenation of surface C species forming CH_x, CO insertion to these CH_x and further hydrogenation of these oxygenates intermediates forming products of C_2 oxygenates [9–11]. The modifications with additives and supports usually facilitate one or more of these steps. Thus the reaction can be directed to oxygenated products.

More than 60 elements from the periodic table had been screened as additives for Rh aiming to improve the activity and selectivity to oxygenates in the 1980s [12]. Combination of Rh, Mn and Li was found to give C_2 oxygenates selectivity up to 70% and STY of C_2 oxygenates 130 g/dm^3 h [13]. However, the catalysts were based on a high loading of Rh 4–5 wt.% [13,14], which was not preferred economically since Rh is a previous metal. Later, an active catalyst containing only around 1 wt.% of Rh was developed at the Dalian Institute of Chemical Physics in China. A bench scale test was carried out using 105 g (200 ml) catalyst 1.0 wt.% Rh-Mn/SiO_2 under 310 °C, 6 MPa and space velocity 40,000 ml/g h. Within 1000 h on stream no deterioration in the activity and selectivity was observed. The STY of C_2 oxygenates was as high as 292 g/kg-cat h [15].

Here we first undertake a brief overview of the catalyst development for syngas conversion to C_2 oxygenates over Rh-based catalysts, mainly on the effects of different additives and supports on the activity and selectivities. Then we focus on our study on the effects of different carbonaceous materials as supports for Rh-based catalysts, which is seldom investigated yet. Carbon is known to exhibit different properties compared to conventional refractory oxides such as Al_2O_3 and SiO_2 [16]. In particular, carbon nanotubes (CNTs) are known with good thermal, mechanical and electron conductive properties, as well as their well defined nanochannel morphology. These channels may provide an intriguing confinement environment for metal catalysts and catalytic reactions not only because of the spatial restriction but also possible modification of the metal catalyst properties due to the unique electron structure of the curved graphene walls [17].

* Corresponding authors. Tel.: +86 411 84379128; fax: +86 411 84694447.
E-mail addresses: panxl@dicp.ac.cn (X. Pan), xhbao@dicp.ac.cn (X. Bao).

0920-5861/$ – see front matter © 2009 Elsevier B.V. All rights reserved.
doi:10.1016/j.cattod.2009.03.004

2. Overview on catalytic conversion of syngas to C_2 oxygenates

2.1. Effects of additives

The most frequently studied additives are oxophilic oxides such as Mo, Zr, Ti, V and Mn [9,18–21]. These additives exist as low valence oxides after reduction, which can improve the activity up to 10 times while retaining or also improving the selectivity to C_2 oxygenates. Sachtler and Ichikawa ascribed the improved activity of the oxophilic metal promoted Rh/SiO_2 catalyst to the formation of a tilted mode of CO adsorption on the Rh surface, which was evidenced by the red shift of IR stretching frequency of the bridge chemisorbed CO [21]. The tilted adsorbed CO dissociated more easily and hence the CO hydrogenation activity was enhanced. Wang et al. proposed that the active site was $(Rh_x^0Rh_y^+)$–O–M^{n+}, wherein a part of Rh was present as Rh^+ and the promoter ion (M^{n+}) was in close contact with these Rh species based on CO-TPD, XPS and EPR results [22]. Moreover, the formation of small clusters of the Rh–Mn mixed oxide increased the dispersion of the Rh component and hence improving the reaction activity.

Promoters such as iron and zinc oxides increase the selectivity to oxygenates while having little effect on the activity [21]. The addition of a very small amount of iron to rhodium catalyst was believed to favor hydrogenation of reaction intermediates resulting in a dramatically increased selectivity to ethanol [23,24]. Guglielminotti et al. proposed that the Rh sites available for CO and H_2 chemisorption decreased upon the addition of iron to Rh/ZrO_2 [25]. At the same time, doubly bonded CO (Rh–CO–Fe) increased. Thus the formation of oxygenate products was favored. Iridium was also reported to promote the selective synthesis of ethanol while retaining the activity of Rh catalyst [13,14]. For example, the selectivity of ethanol increased from 42.2% to 50.7% upon addition of 0.5% Ir to Rh-Ti-Fe/SiO_2 catalyst [14].

The addition of basic metals such as alkali and alkaline earth metals can suppress the methanation reaction and enhance the CO insertion reaction over Rh catalyst. Thus the selectivity of C_2 oxygenates was improved, but usually the activity was lowered [26–28]. The effect of Li promoter was attributed to electron-donation. Wang et al. proposed that the formation of Rh–Mn mixed oxide was inhibited and the concentration of Rh^0 on the surface of SiO_2 increased when Li was added to Rh-Mn catalyst [29]. It was suggested that the effects of multi-component additives can be retained and superimposed if they are added together to Rh catalyst. For example, Luo et al. modified Rh/SiO_2 catalyst by Mn and Li together, which resulted in an improved activity of Rh catalyst, suppressed formation of hydrocarbons and an improved selectivity of oxygenates [30]. The CO conversion increased from 2.6% to 8.7% and the selectivity of C_2 oxygenates from 13.1% to 31.6% when Mn was added to Rh/SiO_2 (1.0 wt.% Rh and 1.0 wt.% Mn) [31]. Upon further addition of Li promoter, the CO conversion decreased to 6.7% while the selectivity to C_2 oxygenates increased to 48.2% and the methane selectivity decreased dramatically from 64.8% down to 41.9%. Even further addition of Fe did not change significantly the selectivity to oxygenates but led to an improved CO conversion and hence offsetting the suppression effect of Li on the activity. The resulting STY of C_2 oxygenates was as high as 457 g/kg-cat h under 320 °C, 3 MPa syngas and GHSV 12,000 h^{-1} in comparison to 270 g/kg-cat h obtained over Rh–Mn/SiO_2 under the same conditions [31]. Nakajo et al. also reported a synergistic effect of combining Ir and Li with Rh–Mn/SiO_2, leading to a significantly improved selectivity of oxygenates without decreasing the yield [13].

2.2. Effects of supports

In addition to the function of dispersing metal particles, supports can also modify the properties of active metal species through interactions. The selectivity of CO hydrogenation depends closely on the chemical nature of the supports. For example, Rh supported on strongly basic oxides such as MgO and ZnO yielded methanol as a major product [32], whereas supports such as SiO_2 and Al_2O_3 favored formation of methane and higher hydrocarbons [33]. Katzer et al. observed that the selectivity to alcohols varied with the basic character of the support [34]. For example, MgO exhibited ca. 90% selectivity to methanol. In addition, TiO_2 supported catalyst gave the highest ethanol selectivity, followed by SiO_2, CeO_2 and Al_2O_3 [34]. Although the exact mechanisms were not clear, the electron withdrawing/donating capability, morphology and dispersion of metal particles, and reducibility of metal species should play important roles due to the nature of the supports.

Silica is the most frequently used support due to its high surface area, high porosity and good stability. Modification of its porosity and surface area can influence the metal dispersion, which in turn modulates the reaction activity and selectivity. Even the granularity of the silica support was reported to affect the CO hydrogenation [35]. For example, Chen et al. observed that the crystallite size distribution was narrower and Rh particles were more homogeneously dispersed when 14–20 mesh silica was used instead of 20–40 mesh as a support for Rh-Mn-Li catalyst [35]. As a result, the STY and selectivity of C_{2+} oxygenates were significantly increased from 338.6 g/kg-cat h and 49.2% to 618.4 g/kg-cat h and 54.6%, respectively. Treatment of silica support with *n*-C1–C5 alcohols also resulted in an enhancement of the STY of C_2 oxygenates by 10–30% depending on the specific alcohol [36]. This was attributed to the improved Rh dispersion and the increased ratio of Rh^+/Rh^0 sites on catalyst surface, which were considered to favor the CO insertion reaction.

Zeolites were also studied as supports for CO hydrogenation to synthesize C_2 oxygenates, e.g. mesoporous MCM-41 (BET surface area of 1200 m^2/g and pore size of 3 nm) [37]. However, the MCM-41-supported Rh-Mn catalyst exhibited a lower ethanol synthesis activity than Rh–Mn/SiO_2 although SiO_2 had a much lower BET surface area of 200 m^2/g. The authors attributed that to less active sites over Rh–Mn/MCM-41 than over Rh–Mn/SiO_2, evidenced by temperature-programmed reaction experiments [37]. Xu et al. studied NaY zeolite as a support for Rh (2.9 wt.% loading) and they found that CO syngas can be converted to C_2 oxygenates with a rather high selectivity (45–56%) without using any other promoters under 1 MPa, 250 °C, $CO/H_2 = 1$ and GHSV = 15,000 h^{-1} [38]. In particular, the selectivity to acetic acid among oxygenates was as high as 90%. They proposed that Rh catalyst was reconstructed to smaller clusters inside the zeolite cages under reaction conditions and Rh clusters were in close contact with carbonyl clusters or carbonyl ions, which could facilitate the CO insertion reaction. In addition, the reaction intermediates acetate groups could also be better stabilized inside the zeolite cages than the mesopores of SiO_2. Therefore, the selectivity to oxygenates particularly acetic acid increased [38].

2.3. CNT-confined Rh-based catalysts

We recently made use of the well defined channel morphology of carbon nanotubes by confining metal particles inside the channels. These channels do not only exert spatial restriction limiting the aggregation of metal particles, but also modifying the redox properties of metal and metal oxide particles. For example, the reduction of iron oxide particles was facilitated inside CNT channels with respect to those dispersed on the outer surface of CNTs and the reduction temperature decreased within smaller nanotubes [39,40]. The improved reducibility was found to favor the formation of iron carbides under Fischer–Tropsch synthesis (FTS) conditions, which was consistent with an earlier study [41].

Iron carbides have been generally recognized to be essential to obtain high FTS activity [42,43]. Our experiments showed that such CNT-encapsulated Fe catalyst indeed exhibited a higher activity in FTS in comparison to the iron particles dispersed on the exterior CNT surfaces [44].

Since syngas conversion to C_2 oxygenates also requires reduced Rh as the active metal catalyst, we studied the effect of confining Rh–Mn bimetal catalysts inside the CNT channels [45]. Here Mn was essential as a promoter to obtain high selectivity for C_2 oxygenates. Interestingly, the inside Rh-Mn catalyst also exhibited an enhanced activity with respect to RhMn particles dispersed on the exterior surfaces of CNTs, although the latter should be more accessible to reactants. TEM characterization of the particle size along reaction time on stream showed that the fresh confined Rh-Mn catalyst had a particle size of 1–2 nm and grew to 4–5 nm after reaction for 120 h. They were not significantly smaller than those of the outside catalysts (2–3 nm for the fresh and 5–8 nm for the used one). However, the activity of the outside catalyst was by far lower than that of the inside one. Therefore, the particle size cannot be the only factor determining the catalytic activity. Furthermore, SBA-15 was chosen as a support for comparison because it has a morphology of straight channels close to CNTs with an average diameter of 6–7 nm and a pore length around 300–600 nm. Such pores should offer a similar dimensional confinement for metal nanoparticles. However, the SBA-15 supported catalyst exhibited a much lower activity than the CNT supported catalyst under the same reaction conditions [45].

In order to understand better the promoting effects of CNTs to the Rh-based catalyst, we choose other carbonaceous materials with different textural properties for comparison against CNTs: carbon black (CB), mesoporous CMK-3 and activated carbon (AC). Among them, CB has rather well graphitized structure. Both CMK-3 and AC have a very high surface area. In addition, CMK-3 has a replica straight channels of SBA-15 because it has been synthesized using SBA-15 as a template. Here we took a known recipe of multi-component promoted Rh catalyst including Mn, Li and Fe [31], as a part of screening for catalysts with a high activity and selectivity of C_2 oxygenates.

3. Experimental

3.1. Preparation of catalysts

CMK-3 was synthesized following the method reported by Ryoo et al. using SBA-15 as a template [46]. AC and CB were purchased from Beijing Guanghua Wood Plant and Aldrich, respectively. The metal recipe known with a high activity and selectivity of C_2 oxygenates contained 1.2 wt.% Rh and the weight ratio of Rh:Mn:Li:Fe was 1:1:0.075:0.05 [31]. The catalysts supported on CB, CMK-3 and AC were prepared by the impregnation technique using aqueous solution of $RhCl_3$, $Mn(NO_3)_2$, $LiNO_3$ and $Fe(NO_3)_3$ mixture. Then they were dried in air for 10 h at 110 °C. The obtained catalysts are denoted as RMLF/CB, RMLF/CMK-3 and RMLF/AC, respectively. For convenience of comparison, here we also listed the data of RMLF/CNTs, which has been reported previously [45].

3.2. Characterization of catalysts

Transmission electron microscopy (TEM) was used to characterize the catalyst morphology and the metal particle size. It was carried out on an FEI Tecnai microscope operated at an accelerating voltage of 120 kV. Prior to TEM measurement, the catalyst was treated in pure H_2 (50 ml/min) for 2 h at 350 °C, which is the same reduction condition applied for catalytic reaction tests. The sample was ultrasonically dispersed in ethanol and placed onto a carbon film supported over a copper grid for TEM measurements. The metal particle size distribution was obtained by measuring at least 150 particles for each catalyst.

Temperature-programmed desorption (TPD) was carried out in a quartz microreactor. The catalyst (50 mg) was reduced in-situ for 2 h at 350 °C in H_2 and then cooled down to room temperature in H_2 flow. Subsequently, the sample was heated in a flowing He stream (30 ml/min) up to 900 °C at a rate of 10 °C/min. Simultaneously, the effluents (m/e = 28.06 for CO, 43.97 for CO_2) were monitored by an online quadruple MS (Balzers, Omni-star 300). MS was calibrated for CO and CO_2 using calcium oxalate and calcium carbonate [47].

X-ray diffraction (XRD) was performed on a Rigaku diffractometer using Cu Kα radiation at room temperature at 40 kV and 150 mA. The textural properties of carbon supports were characterized by N_2 adsorption–desorption at 77 K on the Quantachrome instrumental system. CO chemisorption was performed on the Autosorb-1-C/MS apparatus. Each sample was dried in vacuum for 6 h at 200 °C and reduced in a flowing H_2 for 2 h at 350 °C. Then the sample was evacuated at 10^{-5} Torr for 3 h, followed by cooling down to room temperature. The CO adsorption isotherms were measured at 40 °C. The uptake of CO was used to calculate Rh metal dispersion and particle size, assuming that each surface metal atom adsorbs one CO molecule, i.e. $CO/Rh_{surface} = 1$ [48,23].

3.3. Catalytic reaction

CO hydrogenation was carried out in a fixed-bed microreactor with syngas composition of $H_2/CO = 2$ (volume ratio) and GHSV = 12,000 h^{-1}. Prior to reaction, the catalyst was in situ reduced in a flow of H_2 (50 ml/min) for 2 h at 350 °C. Then the catalyst bed was cooled down to the reaction temperature in H_2 and syngas was introduced. The effluent passed through a condenser filled with cold de-ionized water. The tail gas was analyzed on-line with a Varian CP-3800 GC equipped with a Porapak Q column and a TCD detector. The condensed oxygenate products were analyzed off-line with the same GC (an HP-FFAP capillary column and an FID detector). Selectivity was expressed in C% and formation rate of C_2 oxygenates as space time yield (STY), i.e. g C_2 oxygenates per kg catalyst per h.

4. Results and discussion

Fig. 1 shows the CO conversion and the STY of C_2 oxygenates as a function of reaction temperature in the range of 290–320 °C. It can be seen that both the CO conversion and the C_2 oxygenates yield increase with the increasing temperature on all catalysts. The STY of C_2 oxygenates under the same conditions decreases in a sequence: RMLF/CNTs > RMLF/CB > RMLF/CMK-3 > RMLF/AC. The CO conversion follows a similar sequence, but the CB and CMK-3 supported catalysts exhibit a similar CO conversion. When RMLF/CNTs was tested at a higher pressure (5 MPa), both the CO conversion and STY of C_2 oxygenates increase significantly.

Table 1 lists the product selectivities at 320 °C and 3 MPa. The selectivity of C_{2+} oxygenates on RMLF/CNTs is slightly lower than on the CB supported catalyst, but higher than those on RMLF/CMK-3 and RMLF/AC. The selectivity of CO_2 is similar on the CNTs and CMK-3 supported catalysts, which are higher than those on RMLF/CB and RMLF/AC. Interestingly, formation of the undesirable by-product methane appears to be suppressed over RMLF/CNTs, in that the methane selectivity is the lowest among all catalysts. The methane selectivity versus the catalysts coincidently follows a reverse changing trend to the yield of C_{2+} oxygenates, as shown in Table 1. Thus, it can be seen that CNTs help facilitating CO hydrogenation and selective formation of C_{2+} oxygenates on Rh-based catalyst with respect to other carbonaceous materials.

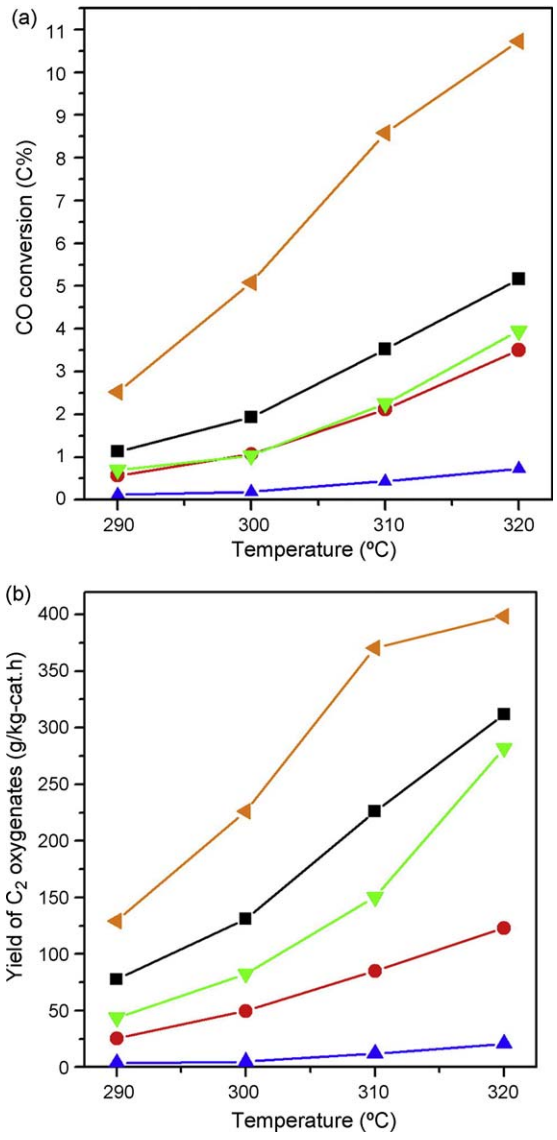

Fig. 1. CO conversion and space time yield of C_2 oxygenates at 3 MPa. (■) RMLF/CNTs [45], (▼) RMLF/CB, (●) RMLF/CMK-3, (▲) RMLF/AC. (◀) RMLF/CNTs at 5 MPa.

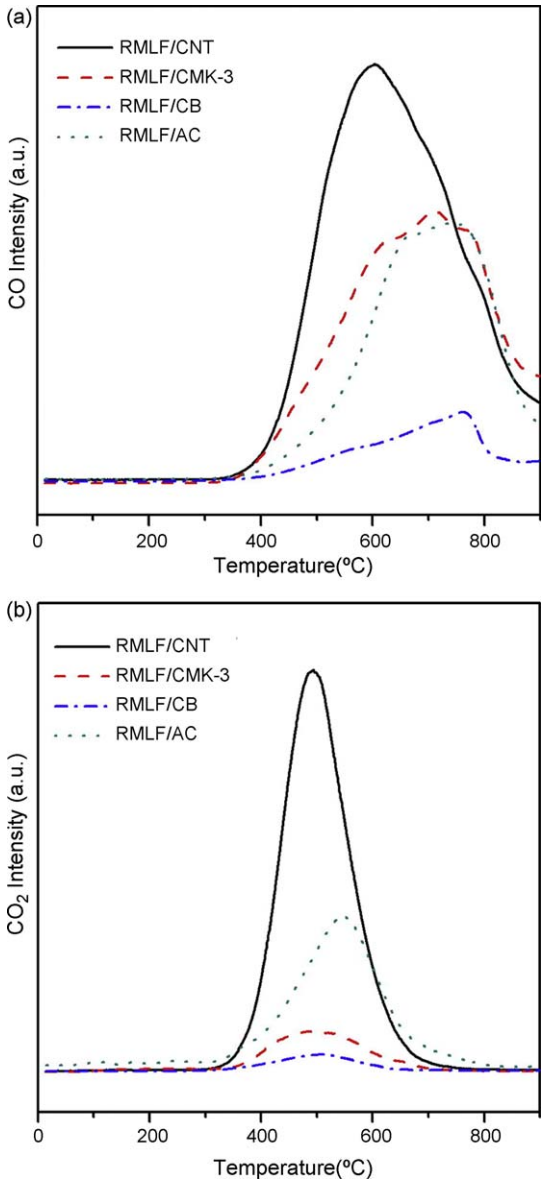

Fig. 2. TPD curves of different catalysts (a) CO and (b) CO_2 peaks detected by MS.

Since these catalysts have the same metal compositions, we first turn our attention to the nature of the carbonaceous materials, which can influence the properties of metal species via metal-support interaction. For example, the metal dispersion is often modified by using supports with different textural properties e.g. surface area, porosity and surface oxygen groups. Fig. 2 shows TPD profiles of reduced catalysts. RMLF/CNTs exhibit a broad and strong CO peak in the range of 400–800 °C accompanied by a weaker CO_2 peak in the range of 350–700 °C. The CO peak in this temperature range was generally assigned to the decomposition of carboxyl/quinone, phenols and ether groups on the surface while the CO_2 peak to the decomposition of carboxylic anhydride and lactone groups [49–51]. Other catalysts also exhibit CO and CO_2 peaks in a similar temperature range but with much weaker intensity. CNTs contain the most amount of surface oxygen groups among all catalysts, as shown in Table 2. CMK-3 and AC have similar amount of them, while CB has the least among all catalysts. These surface oxygen groups on one hand are beneficial for anchoring of metal precursors and on the other hand, may also affect the reaction due to their electron negativity. Considering the activity trend shown in Fig. 1, these surface oxygen groups might not have affected the reaction significantly.

Table 1
CO hydrogenation performance on different catalysts.

Catalyst	CO conv. (C%)	Selectivity of products (C%)				
		[a]$C_{2+\text{-oxy}}$	CH_4	[b]C_{2+}HC	MeOH	CO_2
RMLF/CNTs	5.16	52.4	14.6	12.5	1.5	19.0
RMLF/CB	3.95	59.0	16.2	11.4	2.6	10.8
RMLF/CMK-3	3.5	39.6	27.6	9.2	3.1	20.6
RMLF/AC	0.73	26.8	32.7	15.6	11.3	13.5

Reaction conditions: 320 °C and 3.0 MPa (H_2/CO = 2).
[a] $C_{2+\text{-oxy}}$ denotes oxygenates containing two and more carbon atoms.
[b] C_{2+}HC denotes hydrocarbons containing two and more carbon atoms.

N_2 adsorption–desorption was carried out to characterize the textural properties of the supports and the corresponding supported catalysts. As shown in Table 3, the BET surface areas of CNTs and CB are 228 and 76 m^2/g, respectively. AC and CMK-3 have similar surface areas, as high as ca. 1000 m^2/g. They are much higher than those of CNTs and CB. Furthermore, CNTs have a bimodal pore distribution. The smaller one is in the range of 3–8 nm, consistent with the inner diameters of the nanotubes from

Table 2
Total amounts of surface oxygen groups determined by TPD.

Samples	TPD (μ mol/g)	
	CO	CO_2
RMLF/CNTs	1018.6	100.8
RMLF/CB	110.8	4.2
RMLF/CMK-3	586.2	13.1
RMLF/AC	567.6	45.4

Table 3
Textual properties of carbon supports and the corresponding catalysts obtained by N_2 adsorption–desorption.

Samples	S_{BET} (m^2/g)	V_{tot} (cm^3/g)	Pore diameter (nm)
CNTs	228	0.60	10.5
RMLF/CNTs	213	0.48	9.0
CB	76	0.31	6.5
RMLF/CB	61	0.16	10.7
CMK-3	919	1.01	3.8
RMLF/CMK-3	1237	1.24	4.0
AC	1060	0.54	2.2
RMLF/AC	930	0.45	2.0

the visual observation with TEM (4–8 nm). The larger one is in the range of 20–30 nm, which is formed by the aggregated and tangled CNTs. CB has an average pore size of 6.5 nm. AC contains both micropores and mesopores, and the average pore size is 2.2 nm. CMK-3 is a reverse replica of SBA-15 and its average pore size is 3.8 nm, which is not significantly different from the CNT channel diameter. Upon being loaded with metal components, there is only a slight decrease in the surface area and the pore volume for CNTs, CB and AC, likely due to pore blocking by metal particles. In comparison, those of CMK-3 increase slightly. Li et al. also reported a similar phenomenon for CMK-3 after being loaded with Ru metal [52]. However, the reason is not clear yet.

A support with a high surface area generally favors the dispersion of metal species. This could affect the catalytic conversion of syngas to oxygenates since it is a structure-sensitive reaction [53]. Fig. 3a shows that the particle size of RMLF/CNTs is in the range of 1–2.5 nm (Fig. 4a) measured from TEM. About 80% of these particles are estimated to be located inside the CNT channels, as examined by rotating the TEM specimen against the electron beam [45]. It can be seen from Fig. 3b that CB is mostly composed of carbon spheres and metal particles are uniformly dispersed with a size of 2–4 nm (Fig. 4b). In the sample RMLF/CMK-3, the straight channels in CMK-3 can still be discernible from Fig. 3c although the TEM specimen of RMLF/CMK-3 is not thin enough, which makes the images blurred. The metal particles we can observe are

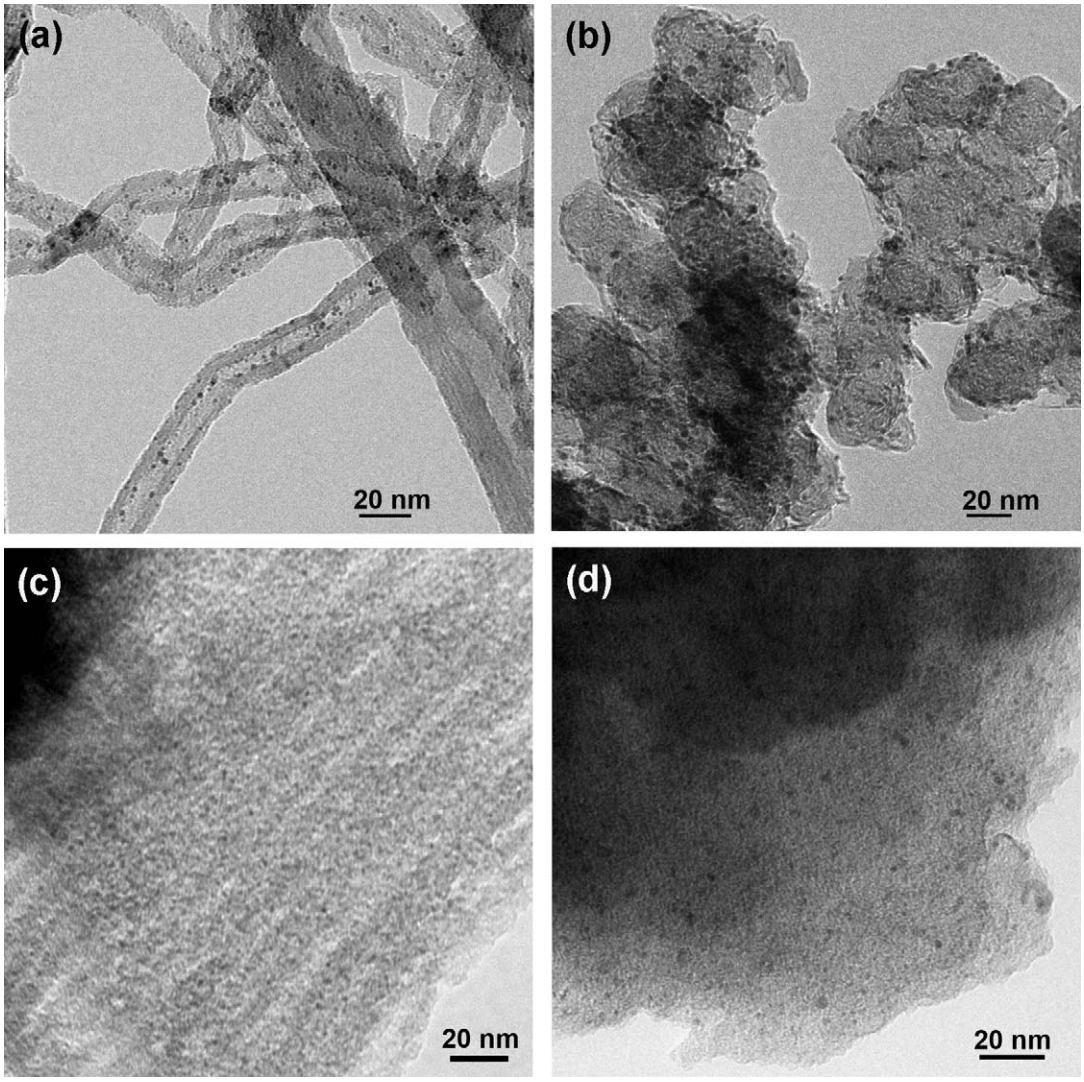

Fig. 3. TEM images (a) RMLF/CNTs, (b) RMLF/CB, (c) RMLF/CMK-3, (d) RMLF/AC.

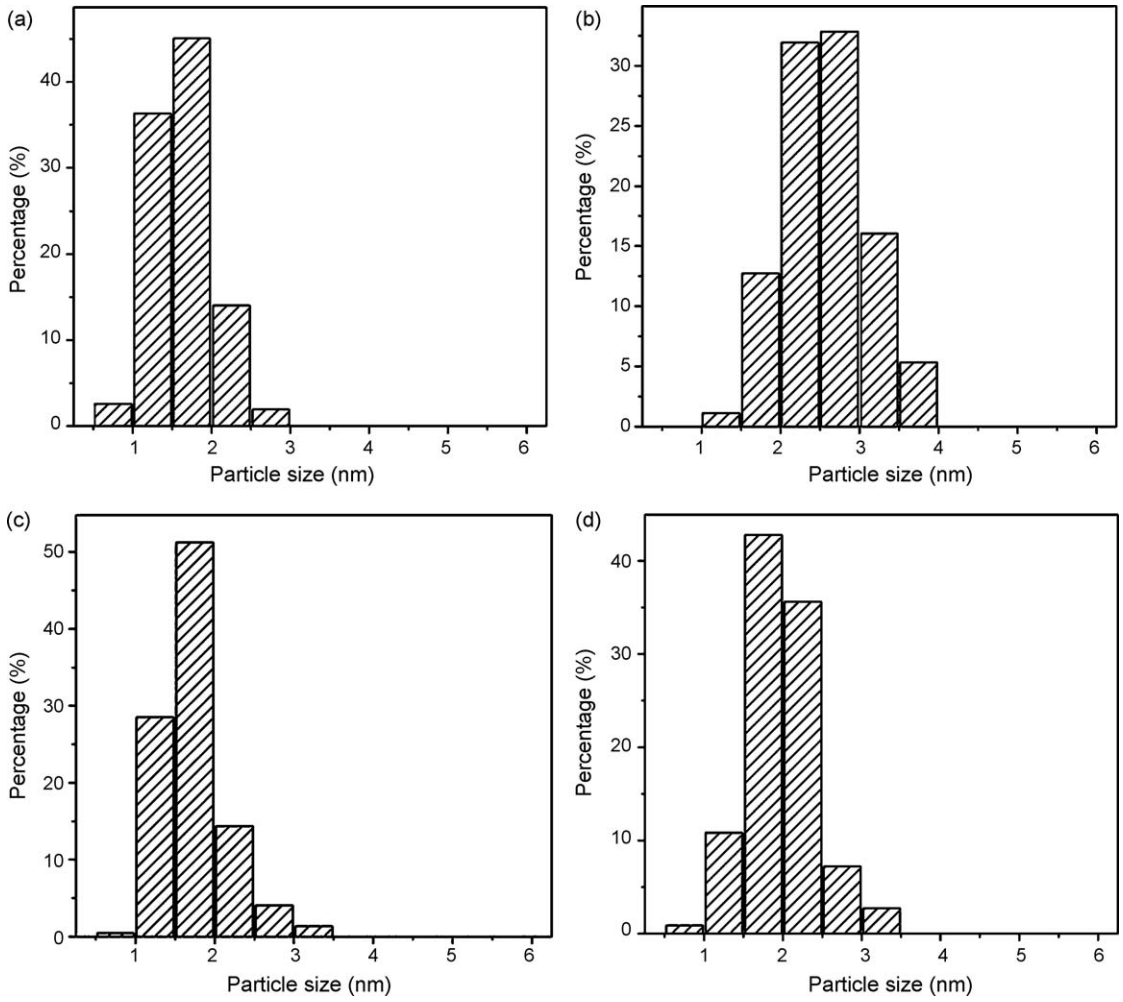

Fig. 4. The particle size distribution measured from TEM (a) RMLF/CNTs, (b) RMLF/CB, (c) RMLF/CMK-3, (d) RMLF/AC.

homogeneously distributed with a size in a range of 1–2.5 nm (Fig. 4c). However, we cannot exclude the possibility of larger particles in the blurred region. On the support of AC, the metal particles are also highly dispersed (Fig. 3c) and the particle size falls in the range of 1–3 nm (Fig. 4d).

However, chemisorption characterization indicates that the metal dispersion and particle size differ among different catalysts, as shown in Table 4. For example, the metal dispersion on CNTs is 21% and on CB 16%. The average particle sizes on CNTs and CB are estimated to be around 5–7 nm, larger than those measured from TEM. RMLF/AC exhibits an extremely high dispersion (89%) and it is much higher than the other catalysts. Surprisingly, Rh is poorly dispersed on CMK-3, although it has a similar surface area as AC. The average particle size of RMLF/CMK-3 is 12.7 nm, which is one order of magnitude larger than that of RMLF/AC. TEM usually gives images of a small fraction of a technical catalyst. There are possibly a few larger particles present around relatively thick areas in the TEM specimen, which have not been observed. In addition, Kishida et al. proposed that some of the Rh particles might be partly or wholly embedded in the supports [54]. These could cause the average particle size obtained from CO chemisorption to be larger than that from TEM measurement. Furthermore, CO can also adsorb non-linearly on Rh surfaces in particular in the presence of additives and supports [55], which may also cause divergence in the particle size measured from TEM and chemisorption.

Table 4
Metal particle size and dispersion measured from TEM and CO chemisorption.

Catalysts	TEM d (nm)	CO chemisorption		
		CO uptake (μmol/g)	Dispersion* (%)	Particle size d (nm)
RMLF/CNTs	1–2.5	25	21	5.1
RMLF/CB	2-4	19	16	6.7
RMLF/CMK-3	1–2.5	10	9	12.7
RMLF/AC	1–3	104	89	1.2

* Assuming $CO/Rh_{surface} = 1$.

Our results suggest that the particle size might play a role in these multi-component promoted Rh catalysts supported on carbon materials. Hanaoka et al. studied a series of Rh/SiO_2 catalysts with the particle size ranging from ca. 1 to 6 nm on CO hydrogenation to oxygenates [56]. It was found that catalysts with the particle size larger than 2.5 nm gave higher activities and selectivities of C_2 oxygenates. This is likely the reason for the very low activity of RMLF/AC. Furthermore, Arakawa et al. reported that high dispersion favored CH_3OH formation and C_2-oxygenated compounds were produced favorably for dispersion around 0.2 [5]. RMLF/CNTs and RMLF/CB, which have metal dispersion close to that value, exhibit higher selectivity of C_{2+} oxygenates than the other two carbon-supported catalysts. However, the trend of CH_4 selectivity here is not consistent with that earlier study.

We further characterized the graphitic structure of the carbon materials with XRD. As shown in Fig. 5, CNTs exhibit diffraction

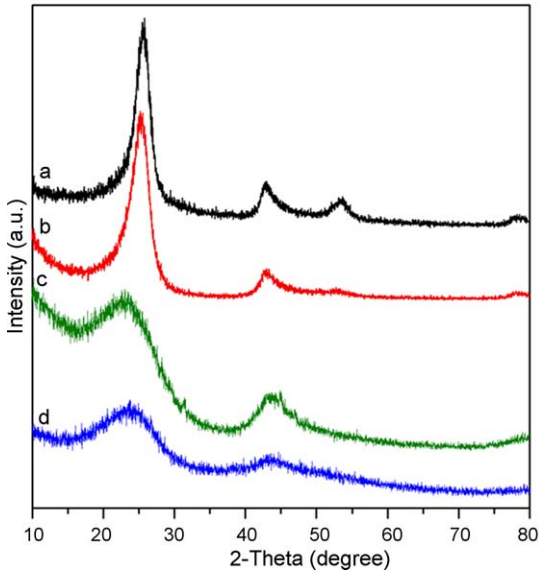

Fig. 5. XRD patterns of carbon materials (a) CNTs, (b) CB, (c) AC, (d) CMK-3.

peaks at 25.7°, 42.8°, 53.5° and 78.1°, which are characteristics of graphitic carbon (JCPDS 656212). This is understandable considering that CNTs are essentially composed of coaxial graphitic cylinders. CB shows similar but slightly broadened diffraction peaks with respect to CNTs. In comparison, the diffraction peaks of both CMK-3 and AC are broadened obviously (Fig. 5c and d), indicating a poorly crystallized graphitic structure. The carbon material graphitized to a higher level would bring about better electron conductivity. This possibly would facilitate the electron transfer between the metal species and CO molecules and hence the CO activation. This could help improving the activity of the CNTs and CB supported catalysts in comparison to CMK-3 and AC.

Furthermore, these carbon materials differ in their morphologies. The previous study showed a promoting effect of CNTs by confining a bimetal RhMn catalyst inside the CNT channels and interactions between metals and the graphene surfaces might be one important reason for the different catalytic activities [45]. However, the STY of C_2 oxygenates on the multi-component catalyst was more than twice as high as the bimetal catalyst [45], indicating strong additional promoting effects of Li and Fe, which might outbalance that of CNTs. In addition, our recent theoretical calculation indicates that the concentrations of CO and H_2 molecules can be localized with a higher concentration inside the CNT channels, which could also help facilitate CO hydrogenation inside the CNT channels than that on the outside [57]. CMK-3 also has a morphology of straight nanochannels although the matrix carbon is almost amorphous [46]. This might be a reason for the higher activity of RMLF/CMK-3 than RMLF/AC.

However, syngas conversion to oxygenates is a complicated process, which involves multi-steps. Promoting Rh with various additives and supports can modify one or more of these steps. In particular, the synergistic interaction between all these promoting components may be different on different carbon supports. This will require further systematic experimental studies, so as to elucidate the promoting nature of these materials for Rh-based catalysts and thus helping design of highly active catalysts for selective synthesis of C_2 oxygenates from syngas.

5. Conclusions

We studied the effects of different carbon materials (CB, CMK-3 and AC) as supports for Rh-based catalysts promoted by multi-component additives (Mn, Li and Fe) for catalyzing syngas conversion to C_2 oxygenates. It appears that there are strong additional promoting effects of Li and Fe compared to the bimetal RhMn catalyst, which might outbalance that of CNTs. Even so, RMLF/CNTs still exhibits a highest activity among the four catalysts. Although Rh is very well dispersed on the high surface area AC, this catalyst exhibits a lowest overall activity and a lowest yield of C_2 oxygenates. In addition, the results suggest that combination of the nanochannels and graphitic structure may also play an important role in promoting this reaction in addition to the metal dispersion and particle size in these multi-component promoted Rh catalysts.

Acknowledgment

The work was financially supported by National Natural Science Foundation of China (project no. 20503033).

References

[1] M. Asif, T. Muneer, Renew. Sust. Energy Rev. 11 (2007) 1388.
[2] A.E. Farrell, R.J. Plevin, B.T. Turner, A.D. Jones, M. O'Hare, D.M. Kammen, Science 311 (2006) 506.
[3] V. Subramani, S.K. Gangwal, Energy. Fuels 22 (2008) 814.
[4] M.M. Bhasin, G.L. O'Connor, Belgian Patent, 824822 (1975).
[5] H. Arakawa, K. Takeuchi, T. Matsuzaki, Y. Sugi, Chem. Lett. 13 (1984) 1607.
[6] S.S.C. Chuang, G. Srinivas, M.A. Brundage, Energy Fuels 10 (1996) 524.
[7] R. Burchand, M.J. Hayes, J. Catal. 165 (1997) 249.
[8] B.J. Kip, P.A.T. Smeets, J.H.M.C. Van Wolput, H.W. Zandbergen, J. Van Grondelle, R. Prins, Appl. Catal. 33 (1987) 157.
[9] M. Ichikawa, T. Fukushima, J. Chem. Soc., Chem. Commun. (1985) 321.
[10] A. Takeuchi, J.P. Katzer, J. Phys. Chem. 86 (1982) 2438.
[11] S.S.C. Chuang, R.W. Stevens Jr., R. Khatri, Top. Catal. 32 (2005) 225.
[12] Y. Yoneda, Progress in C1 Chemistry in Japan, Elsevier, Amsterdam, 1989.
[13] T. Nakajo, K.I. Sano, S. Matsuhira, H. Arakawa, J. Chem. Soc., Chem. Commun. (1987) 647.
[14] H. Arakawa, T. Fukushima, M. Ichikawa, S. Natsushita, K. Takeuchi, T. Matsuzaki, Y. Sugi, Chem. Lett. 14 (1985) 881.
[15] P.Z. Lin, D.B. Liang, H.Y. Luo, C.H. Xu, H.W. Zhou, S.Y. Huang, L.W. Lin, Appl. Catal. A 131 (1995) 207.
[16] J. Phillips, J. Weigle, M. Herskowitz, S. Kogan, Appl. Catal. A 173 (1998) 273.
[17] A.N. Khlobystov, D.A. Britz, G.A.D. Briggs, Acc. Chem. Res. 38 (2005) 901.
[18] J. Kowalski, G.V.D. Lee, V. Ponec, Appl. Catal. 19 (1985) 423.
[19] H.Y. Luo, H.W. Zhou, L.W. Lin, D.B. Liang, J. Catal. 145 (1994) 232.
[20] A.S. Lisitsyn, S.A. Stevenson, H. Knözinger, J. Mol. Catal. 63 (1990) 201.
[21] W.M.H. Sachtler, M. Ichikawa, J. Phys. Chem. 90 (1986) 4752.
[22] Y. Wang, H.Y. Luo, D.B. Liang, X.H. Bao, J. Catal. 196 (2000) 46.
[23] M.M. Bhasin, W.J. Bartley, P.C. Ellgen, T.P. Wilson, J. Catal. 54 (1978) 120.
[24] V. Schünemann, H. Treviño, G.D. Lei, D.C. Tomczak, W.M.H. Sachtler, K. Fogash, J.A. Dumesic, J. Catal. 153 (1995) 144.
[25] E. Guglielminotti, F. Pinna, M. Rigoni, G. Strukul, L. Zanderighi, J. Mol. Catal. 103 (1995) 105.
[26] S.C. Chuang, J.G. Goodwin Jr., I. Wender, J. Catal. 95 (1985) 435.
[27] H. Orita, S. Naito, K. Tamaru, Chem. Lett. (1983) 1161.
[28] S. Kesraoui, R. Oukaci, D.G. Blackmond, J. Catal. 105 (1987) 432.
[29] Y. Wang, Z. Song, D. Ma, H.Y. Luo, D.B. Liang, X.H. Bao, Appl. Catal. A 149 (1999) 51.
[30] H.Y. Luo, P.Z. Lin, S.B. Xie, H.W. Zhou, C.H. Xu, S.Y. Huang, L.W. Lin, L.B. Liang, P.L. Yin, Q. Xin, J. Mol. Catal. A 122 (1997) 115.
[31] H.M. Yin, Y.J. Ding, H.Y. Luo, H.J. Zhu, D.P. He, J.M. Xiong, L.W. Lin, Appl. Catal. A 243 (2003) 155.
[32] M. Ichikawa, Bull. Chem. Soc. Jpn. 51 (1978) 2268.
[33] X.D. Xu, E.B.M. Doesburg, J.J.F. Scholten, Catal. Today 2 (1987) 125.
[34] J.R. Katzer, A.W. Sleight, P. Gajardo, J.B. Michel, E.F. Gleason, S. McMillan, Faraday Discuss. Chem. Soc. 72 (1981) 121.
[35] W.M. Chen, Y.J. Ding, D.H. Jiang, Z.D. Pan, H.Y. Luo, Catal. Lett. 104 (2005) 177.
[36] D.H. Jiang, Y.J. Ding, Z.D. Pan, W.M. Chen, H.Y. Luo, Catal. Lett. 121 (2008) 241.
[37] H.M. Ma, Z.Y. Yuan, Y. Wang, X.H. Bao, Surf. Interface Anal. 32 (2001) 224.
[38] B.Q. Xu, K.Q. Sun, Q.M. Zhu, W.M.H. Sachtler, Catal. Today 63 (2000) 453.
[39] W. Chen, X.L. Pan, M.G. Willinger, D.S. Su, X.H. Bao, J. Am. Chem. Soc. 128 (2006) 3136.
[40] W. Chen, X.L. Pan, X.H. Bao, J. Am. Chem. Soc. 129 (2007) 7421.
[41] C. Wang, Q.X. Wang, X.D. Sun, L.Y. Xu, Catal. Lett. 105 (2005) 93.
[42] G.B. Raupp, W.N. Delgass, J. Catal. 58 (1979) 348.
[43] H. Jung, W.J. Thomson, J. Catal. 134 (1992) 654.
[44] W. Chen, Z.L. Fan, X.L. Pan, X.H. Bao, J. Am. Chem. Soc 130 (2008) 9414.
[45] X.L. Pan, Z.L. Fan, W. Chen, Y.J. Ding, H.Y. Luo, X.H. Bao, Nat. Mater. 6 (2007) 507.
[46] S. Jun, S.H. Jo, R. Ryoo, M. Kruk, M. Jaroniec, Z. Liu, T. Oshuna, O. Terasaki, J. Am. Chem. Soc. 122 (2000) 10712.
[47] F. Coloma, A. Sepúlveda-Escribano, J.L.G. Fierro, F. Rodríguez-Reinoso, Appl. Catal. A 150 (1997) 165.

[48] J.Z. Luo, L.Z. Gao, Y.L. Leung, C.T. Au, Catal. Lett. 66 (2000) 91.
[49] J.L. Figueiredo, M.F.R. Pereira, M.M.A. Freitas, J.J.M. Órfão, Carbon 37 (1999) 1379.
[50] S. Haydar, C. Moreno-Castilla, M.A. Ferro-García, F. Carrasco-Marín, J. Rivera-Utrilla, A. Perrard, J.P. Joly, Carbon 38 (2000) 1297.
[51] S. Kundu, Y.M. Wang, W. Xia, M. Muhler, J. Phys. Chem. C 112 (2008) 16869.
[52] L. Li, Z.H. Zhu, Z.F. Yan, G.Q. Lu, L. Rintoul, Appl. Catal. A 320 (2007) 166.
[53] L. Guczi, Z. Schay, K. Matusek, I. Bogyay, Appl. Catal. 22 (1986) 289.
[54] M. Kishida, K.I. Ichiki, T. Hanaoka, H. Nagata, K. Wakabayashi, Catal. Today 45 (1998) 203.
[55] G. Lafaye, C. Mihut, C. Especel, P. Marécot, M.D. Amiridis, Langmuir 20 (2004) 10612.
[56] T. Hanaoka, H. Arakawa, T. Matsuzaki, Y. Sugi, K. Kanno, Y. Abe, Catal. Today 58 (2000) 271.
[57] J. Guan, X.L. Pan, X. Liu, X.H. Bao, under review.